Jun 28th, 1:30 PM

Visual and Photogrammetric Observations of an Internal Erosion Failure

T. L. Wahl
Bureau of Reclamation, twahl@usbr.gov

R. V. Rinehart
Bureau of Reclamation

M. J. Klein
Bureau of Reclamation

J. B. Rittgers
Bureau of Reclamation

Recommended Citation

Wahl, T., Rinehart, R., Klein, M., Rittgers, J. (2016). Visual and Photogrammetric Observations of an Internal Erosion Failure. In B. Crookston & B. Tullis (Eds.), Hydraulic Structures and Water System Management. 6th IAHR International Symposium on Hydraulic Structures, Portland, OR, 27-30 June (pp. x-x). doi:10.15142/T3370628160853 (ISBN 978-1-884575-75-4).

6th International Symposium on Hydraulic Structures and Water System Management
Portland, Oregon, USA, 27-30 June 2016
ISBN 978-1-884575-75-4 DOI: 10.15142/T3370628160853

Visual and Photogrammetric Observations of an Internal Erosion Failure

T.L. Wahl, R.V. Rinehart, M.J. Klein, J.B. Rittgers[1]
[1]Bureau of Reclamation
P.O. Box 25007
Denver, CO 80225
USA
E-mail: twahl@usbr.gov

ABSTRACT

A 0.91-m (3-ft) high, homogeneous, silty clay embankment was tested to investigate erosion processes occurring during failure by internal erosion. The embankment was constructed in a 3.79-m (12.44-ft) wide test flume equipped with a clear acrylic viewing window at the abutment where failure was initiated. Failure was initiated at mid-height when an embedded 12-mm (½-inch) diameter rebar was removed from the embankment. The test lasted approximately 48 minutes, and during that time the erosion pipe enlarged dramatically. The test was stopped just before the collapse of the soil bridge over the enlarged pipe.

Erosion was visually monitored during the test with video cameras and arrays of still cameras imaging the top of the embankment and the visible abutment. Still photos provided time-lapse imagery and were also used to develop a time-lapse 3D photogrammetric model of the developing erosion channel with estimated areal extents of erosion. Water levels and flow rates were also measured during the test, and data were recorded from an array of geophysical sensors installed on the embankment crest and downstream surface. The embankment materials were characterized before and during construction with in situ measurements of water content, dry density, and erodibility. Visual observations and recorded imagery showed complex flow structures and erosion patterns that are typically not incorporated into current idealized numerical simulation models of the breach erosion process.

Keywords: *Internal erosion, dam breach, physical modeling, numerical modeling, photogrammetry*

1. INTRODUCTION

The ability to model erosion and breaching processes of embankment dams is crucial for making accurate predictions of potential flooding and planning the emergency response to a potential dam failure. Models for simulating dam failure have become more physically based in recent years, especially for failures initiated by overtopping flow. Some physically-based models (e.g., EMBREA and WinDAM C) also now have the capability to simulate failures resulting from internal erosion. During the past two decades there have been several large-scale (2- to 6-m high) outdoor laboratory tests of overtopping-initiated failures of homogeneous embankments that have helped increase understanding of the important erosion mechanisms in that failure mode; these tests have helped to guide the development of mathematical models of the dominant processes for breach development due to overtopping flow. Testing of internal erosion failures has been more limited thus far, as has testing of zoned embankment configurations. Some of the notable efforts in these areas have been those of the Agricultural Research Service hydraulics laboratory at Stillwater, Oklahoma (Hanson et al. 2010) and the testing conducted in Norway in the early 2000s during the European IMPACT project (Lovell 2004; Lovell and Vaskinn 2003; Lovell et al. 2002; Hassan and Morris 2008).

1.1. Purpose

The Bureau of Reclamation has worked for many years to improve capabilities for modeling embankment failure, with initial emphasis on dams impounding water storage reservoirs, and more recently also considering canal embankments (Wahl and Lentz 2011). Because internal erosion is an important failure mode in both environments, Reclamation has also been interested recently in new instrumentation and monitoring techniques that can provide

early detection of seepage or internal flow that could eventually develop into an embankment breach. To address both of these objectives, Reclamation's Dam Safety Technology Development Program is funding laboratory tests aimed at improving the understanding of embankment erosion processes while also providing an environment in which new geophysically-based internal flow detection methods can be tested. This program is intended to eventually include tests of zoned embankments, but the first test conducted in the program was an internal erosion failure of a homogeneous silty clay embankment. The Nuclear Regulatory Commission is also a partner in this research, with a specific interest in zoned and rockfill dams.

2. TEST FACILITY

A new test facility was constructed in Reclamation's indoor hydraulic laboratory in Denver, Colorado in late 2014. The facility provides a 3.79-m (12.44-ft) wide embankment test section in a headbox that is elevated above a large tailbox intended to capture the flow released during a breach test (Figure 1). Capturing the entire flow volume allows sediment to be retained and settled out before water is returned to the lab sump, minimizing the impact on other lab operations. The finite volume of the tailbox limits the total testing time to a few minutes once a breach has enlarged significantly. For tests involving relatively clean embankment soils, flow can be released out the tailwater box back to the lab sump through a spillway section, allowing tests to be run for a longer time period.

Sidewalls of the embankment test section are constructed with a 1H:10V slope to allow for effective compaction of embankment materials against the abutments. The left side abutment is constructed from 19-mm (3/4-in.) thick acrylic to allow viewing of erosion processes during a test.

Figure 1. Embankment breach test facility viewed from the upstream end of the headbox, overlooking the completed test embankment.

3. EMBANKMENT CONSTRUCTION

The embankment was constructed beginning about June 17, one week before the test date of June 25, 2015. Soils were stockpiled in the laboratory and moisturized before placing them into embankment lifts that averaged about 10-15 cm (4-6 in.) compacted thickness. Compaction was accomplished using a pneumatic hammer with a circular foot approximately 15 cm in diameter, with the soil surface covered during compaction by a conveyor belt blanket to help distribute compaction energy. When the embankment was constructed to about 50% of the desired final height, an in situ submerged jet erosion test (ASTM D5852) was run to measure soil erodibility properties and a sand cone density test (ASTM D1556) was performed to evaluate density and water content (Figure 2). The rebar that would be withdrawn to initiate flow and erosion was also placed at the left abutment. A second sand cone test was run at an elevation of 0.76 m (2.5 ft), just before reaching the final height of 0.91 m (3 ft). Water contents were measured periodically from the moisturized soil stockpile throughout construction. The final crest thickness of the embankment was 0.30 m (1 ft), and upstream and downstream slopes were 2H:1V. The crest length of the finished embankment was 3.97 m (13.04 ft).

Figure 2. Sand cone (foreground) and submerged jet erosion tests (back, left) underway during a pause in embankment construction.

3.1. Soil Properties

The soil used to construct the embankment was obtained from a former borrow area for Reclamation's Bonny Dam, about 21 miles north of Burlington, CO. Prior to the start of embankment construction, soil samples were sent to an outside lab for index properties testing. The soil was classified as silty clay (CL-ML), with the following properties:

- 89% fines,
- 11% sand,
- 8% clay (finer than 0.002 mm),
- liquid limit, LL=27,
- plasticity limit, PL=21,
- plasticity index, PI=6,
- optimum water content = 17% (standard Proctor), and
- $\gamma_{d,max}$ = 1.685 g/cm^3 (105.2 lb/ft^3).

Submerged jet erosion tests (ASTM D5852; Hanson and Cook 2004) were performed on the soil specimens created during the standard Proctor compaction test. This test measures soil erodibility by directing a submerged 6-mm (¼-in.) diameter jet at the soil surface to create a scour hole. The observed scour depth versus time data are used to determine the basic parameters (k_d, τ_c) of the linear excess stress equation used to model soil erosion rate:

$$\varepsilon_r = 10^{-4} k_d (\tau - \tau_c) \tag{1}$$

where ε_r is the soil erosion rate (cm/s), k_d is the detachment rate coefficient [cm^3/(N-s)], τ is the applied hydraulic shear stress (Pa), and τ_c is the critical shear stress (Pa) needed to initiate erosion.

The sand cone test performed at mid-height of the embankment showed that the water content was close to optimum (17.3%) and compaction was very effective with a density that was 98% of the standard Proctor maximum value. The second sand cone test performed near the top of the embankment showed somewhat drier compaction conditions (water content = 15.6%) and a lower density, about 93.5% of maximum. Jet test results from the compaction test specimens and the in situ test at mid-height of the embankment are shown in Figure 3. The k_d value [10 cm^3/(N-s)] obtained in the in situ test at mid-height indicates a soil that is very erodible (Hanson and Simon 2001), despite the good compaction achieved at that level.

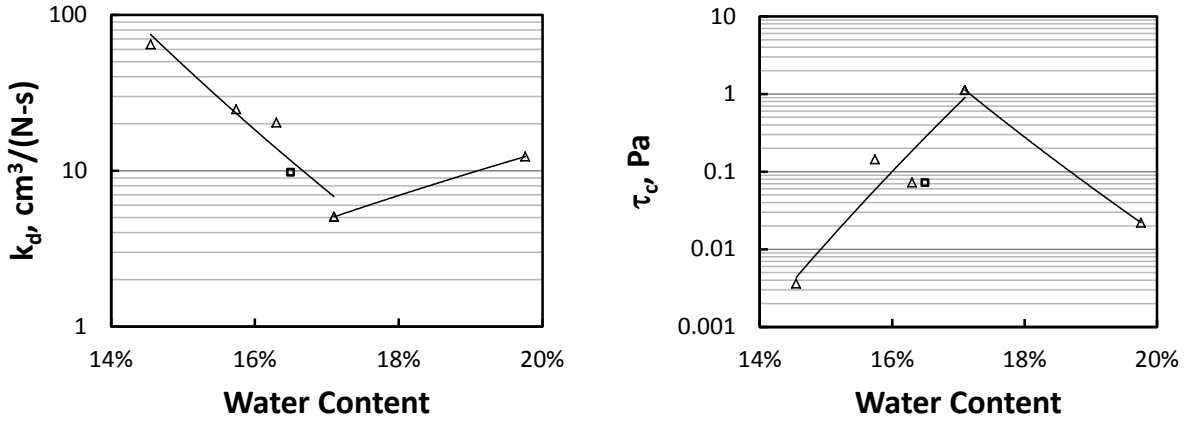

Figure 3. Detachment rate coefficients (k_d) and critical shear stresses (τ_c) determined from submerged jet erosion tests (□ = in situ, Δ = compaction-test specimens), with trend lines shown for dry- and wet-of-optimum water contents.

4. INSTRUMENTATION

4.1. Hydraulic Measurements

Flow into the headbox is measured by the laboratory's fixed set of venturi flow meters. The facility was designed with the intention for tests to be run with a constant, large inflow rate. Most of the inflow in the early stages of a test is spilled out of the headbox through a spillway section with a crest elevation that can be increased during a test by dropping stoplogs into place. This allows a relatively constant upstream head to be maintained during the early stages of breach initiation. Flows through the spillway section are measured by a long-throated flume so that net breach outflow discharges can be calculated.

During the earliest phases of breach initiation, when flow through a developing internal erosion channel might be very small, there is insufficient accuracy in the venturi meter and flume measurements of inflow and spillway flow to allow good estimation of flows through the embankment. During this phase, flows through the embankment are directed to a small supercritical flow flume.

4.2. Imaging

Two arrays of still photo cameras were used to record images of the internal erosion taking place at the left abutment of the embankment test section and any headcut erosion taking place on the downstream slope of the embankment. Eight cameras were set up to take photos through the acrylic abutment wall, and 6 cameras were positioned overhead to obtain photos of the surface of the left end of the embankment. Each camera's field of view included photogrammetry targets to enable subsequent image analysis. The 14 cameras were synchronized together to collect simultaneous images at 10 second intervals during the test. Following the completion of test, these images were processed to create time-lapse three-dimensional photogrammetry models of the observed erosion channels (i.e., 4D photogrammetry).

Additional still cameras were set up at two different downstream viewing positions during the construction of the test facility and during the first test to record time-lapse progress of construction activities and the breach test. Video cameras also recorded the test from 2 locations, one viewing the downstream embankment slope and the other viewing the left abutment through the acrylic window.

4.3. Geophysical Sensors

Approximately 24 hours before the test, several surface-mounted geophysical sensors were installed across the crest and downstream face of the embankment. Two general types of geophysical sensors were installed: vertical-axis seismic sensors (geophones), and passive electrical sensors (non-polarizable self-potential electrodes). Passive electrical (self-potential) data were collected using a medical research-grade, 32-channel, 24-bit electroencephalography data acquisition system manufactured by the Dutch company BioSemi B.V. Passive seismic data were collected using an industry-standard, 24-channel, 24-bit seismograph manufactured by Geometrics, Inc.

In addition to wired passive seismic data collection, two different wireless sensor network (WSN) prototypes were deployed across the embankment crest, each with seven seismic sensors installed coincident with the wired seismic sensors. This was done in collaboration with Colorado School of Mines (CSM) researchers, in order to conduct a side-by-side comparative analysis of the wired and wireless passive seismic data characteristics, and to test the functionality and robustness of the two WSN prototype systems for infrastructure monitoring applications.

Baseline (passive) geophysical data were collected using each data acquisition system, prior to filling the reservoir with water, and after reservoir filling but before the initiation of erosion. Continuous passive monitoring data were simultaneously collected using all four systems throughout the entirety of the piping failure experiment. Data collection started just prior to the filling of the upstream reservoir and continued until the test was completed and the upstream reservoir was emptied.

The main goals of geophysical data analysis are to 1) identify characteristic data signatures associated with the initiation, progression and location of the induced piping feature, 2) to develop and/or test various techniques for imaging the piping feature (e.g., position, orientation, depth, lateral extent, etc.) using the passive monitoring data alone, and 3) to compare the quality of passive seismic data recorded with the prototype WSN devices. Additionally, we plan to collaborate with CSM researchers to test various trained and untrained machine learning algorithms and their usefulness in identifying anomalous or undesirable embankment behavior (e.g., piping features/progression of embankment failure) from the passive geophysical data.

5. TEST OBSERVATIONS

The test was started with an inflow of 0.45 m^3/s (16 ft^3/s) established into the model headbox. Stoplogs on the headbox spillway were adjusted to bring the water surface up to about 75 mm (3 in.) from the crest of the embankment, or about 8% freeboard. The rebar was withdrawn from the embankment using a manual winch. Water levels in the headbox, tailbox, and at the spillway flume were recorded during the test by an automated data acquisition system. Flow measurements at the supercritical flow flume were made manually for the first few

minutes of the test. Unfortunately, a cleat temporarily installed during embankment construction was found left in place and within a few minutes it began to prevent the flow from cleanly entering the supercritical flume. This fact, along with some calibration problems related to water levels sensors and the long throated flume in the spillway channel, prevented accurate breach channel flow rate data from being obtained during the test. Fortunately, photo, video, and geophysical data was collected quite successfully during the test. The photo and video records provided interesting insights about flow mechanisms and erosion processes. The geophysical data are not presented in this paper.

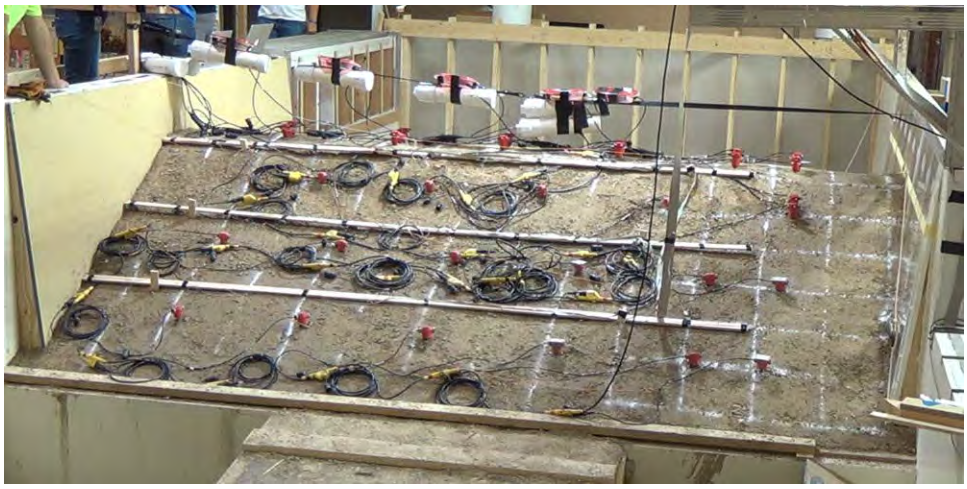

Figure 4. Geophysical sensors installed on the crest and downstream slope of the embankment.

Erosion of the internal channel (pipe) created by removal of the rebar started immediately, indicated by muddy water exiting onto the downstream slope of the embankment. However, the erosion channel was not visible against the clear acrylic abutment wall until about 3-4 minutes after removal of the rebar. For about 15 minutes the erosion channel appeared to enlarge uniformly along its length. As the height of the eroded channel approach one half of the upstream head above the invert of the channel, accelerated scour of the floor of the channel began just downstream from the entrance (Figure 5). The mechanism driving this appeared to be a strong counter-rotating eddy in the channel entrance created by streamlined flow entering the floor of the channel and a strong contraction from the roof of the entrance, where water from the upper part of the reservoir needed to turn a greater than 90º corner to enter the channel (Figure 6). The flow structure was very similar to that of a submerged hydraulic jump that might be observed downstream from a partially open sluice gate. Coincident with formation of this scour in the floor of the entrance, accelerated scour of the roof of the channel began about 4-5 diameters further downstream, seemingly due to a deflection of flow out of the scour hole and up toward the roof. For several minutes a system of stationary, alternating vortices persisted in the enlarging eroded channel. As the channel enlarged further, this flow structure broke down and seemed less dominant.

The test was stopped after about 48 minutes due to the tailbox filling to its capacity. After flow was shut off and the reservoir had drained, it became evident that horizontal enlargement of the channel had also been very significant, especially around the entrance to the channel (Figure 7). The width of the eroded channel was much greater just inside the entrance than it was at the opening visible from the upstream side of the embankment (Figure 8). Distinct lift lines were visible in the eroded channel walls and erosion had either accelerated along weak layers or was just generally more rapid in a horizontal direction, perhaps due to non-isotropic compaction structure of the soil. The three-dimensional nature of the flow approaching the channel entrance may have also contributed to a difference in horizontal and vertical erosion rates. There was a large overhang at the entrance to the eroded channel with the widest eroded section being near the invert of the channel. It appeared that lateral flow along the embankment face had created a vortex in the entrance of the channel that accelerated lateral erosion of the channel (Figure 9). This flow structure seems similar to that observed by other investigators during the later stages of breach widening (e.g., in fuse plug embankment erosion tests by Pugh [1985]). Here, there seems to be evidence that such a structure may be important even before the breach has fully formed and moved into the dominantly widening phase.

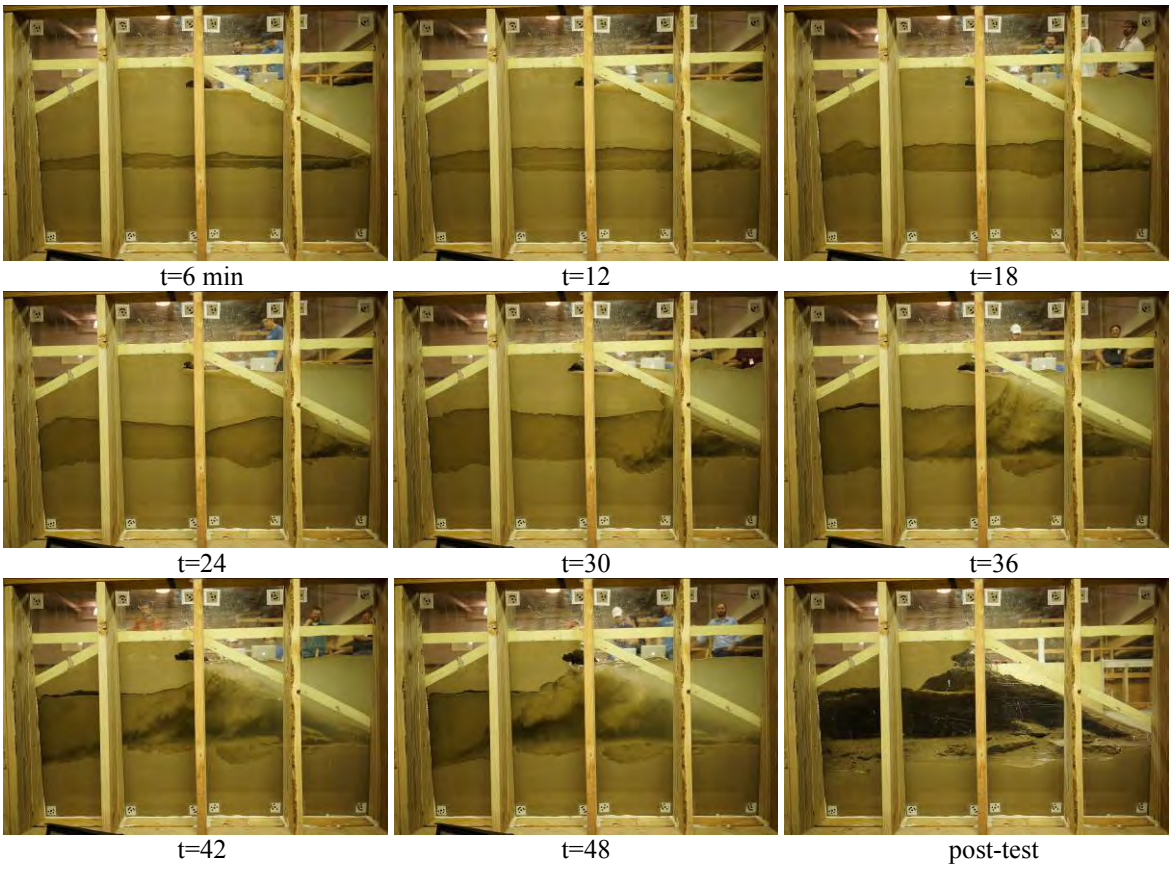

Figure 5. Time lapse photos at 6 minute intervals. The photos show progressive development of the internally eroded flow passage. Note the structure of the flow that leads to development of an enlarged chamber at the upstream end of the conduit. The final photo was taken after the headbox had drained.

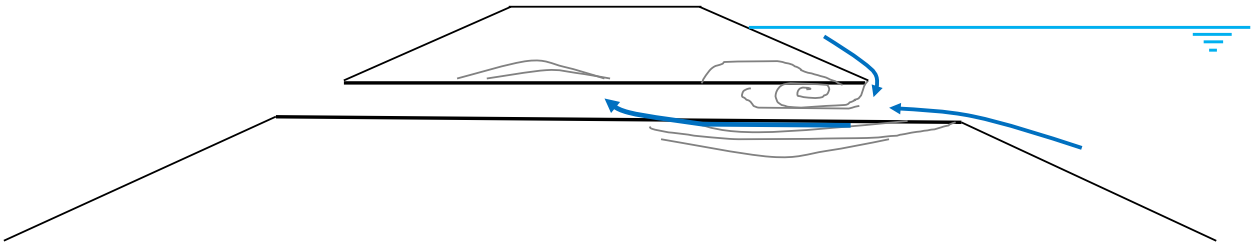

Figure 6. Sketch showing flow structure and related erosion patterns observed during internal erosion test.

One flow feature that was unexpectedly absent from the test was significant headcut erosion where the flow exited the internal erosion channel onto the downstream slope of the embankment. This has been a feature of some previous erosion tests involving piping of relatively weak soils (Hanson et al. 2010). However, in this test, there was very little downward erosion of the downstream slope. This is believed to be due, at least in part, to the fact that the lower half of the embankment seemed to be better compacted than the upper half, based on the sand cone density test results. This may have been due to a combination of lower water content and the natural difficulty of compacting the lifts as the embankment grew taller and narrower. Erosion of the internal channel also seemed to take place mostly in the upward direction. One other possible factor in this is the contribution of gravity forces to destabilizing the roof of the channel. Since this soil was relatively weak (even where well compacted) as shown by the erodibility tests, the gravitational contribution could have been relatively significant, leading to more rapid upward growth of the erosion channel.

Figure 7. Post-test photo illustrating significant widening of the erosion channel, especially near its base.

Figure 8. Post-test overhead view of the entrance to the internal erosion flow channel.

5.1. Photogrammetry

Following completion of the test, approximately 120 GB of fixed camera imagery was processed to create 4D photogrammetry models of the erosion visible through the clear abutment wall and on the downstream slope (4D=3 spatial dimensions plus time). Two images from the abutment model are shown in Figure 10. At each time step, flow cross-sectional areas of the eroded channel were calculated. These data will be valuable for making later comparisons to numerical model simulations of the test.

6. DISCUSSION

The primary purpose for the visual observations and photogrammetric data reported here has been to improve the qualitative understanding of important physical processes and mechanisms during internal erosion leading to dam breach. To make practical use of these tests, we must consider scale effects that might lead the model structures to behave differently from prototype-scale structures.

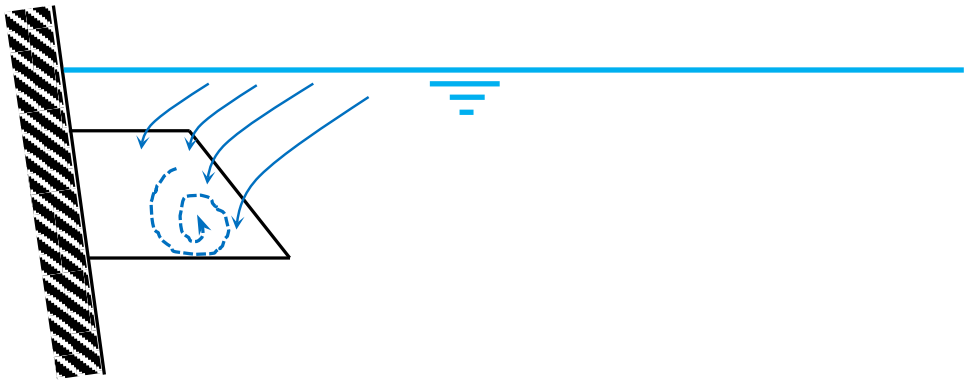

Figure 9. Sketch showing an idealized view of the flow, looking downstream during enlargement of the internal erosion flow channel. This type of vortex formation may lead to accelerated widening of the base of the channel.

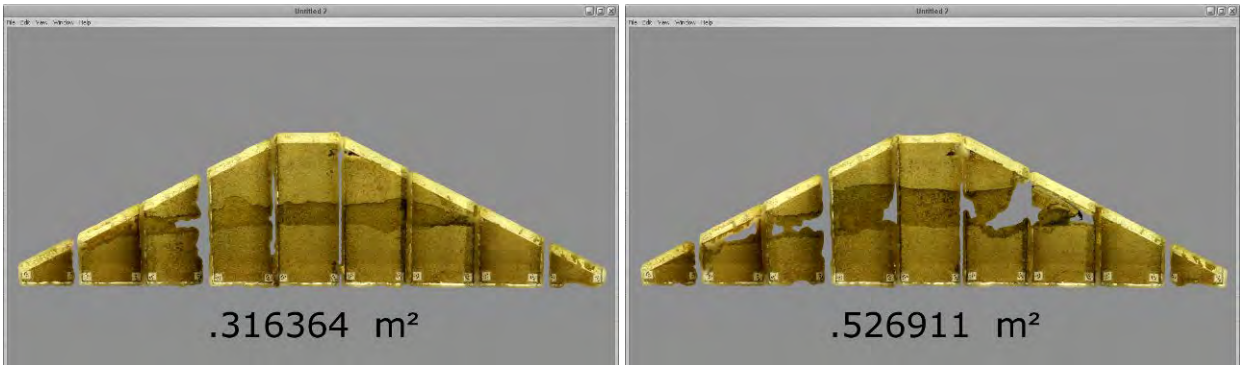

Figure 10. Two images from the 4D photogrammetry model of the internal erosion flow channel. In blanked-out (gray) areas the model was not able to resolve the far side of the channel due to turbidity or other image quality problems.

The dominant physical processes during enlargement of the internal channel penetrating the embankment are gravity-driven flow through the channel and erosion of the channel boundaries through a process of soil detachment from the flow surfaces. Although sediment detached from the boundaries must be transported out of the channel, it is likely that the transport capacity of the flow far exceeds the detachment rate, so the detachment rate should limit the erosion process. For a scale model to faithfully represent the flow processes, the ratio of flow inertial forces and gravitational forces (the Froude number) must be the same in the model and prototype. For a model to faithfully represent the soil detachment process, the ratio of flow forces causing detachment and soil forces resisting detachment must also be the same. Further complicating matters, it is not fully clear whether the flow forces causing detachment are more closely related to the inertia of the flow or the viscous properties of the fluid. The fact that Eq. 1 utilizes shear stress implies the latter, but we can easily imagine that the inertia of flow against a protruding soil element could also lead to detachment of that soil mass. Clearly, it is impossible to maintain all of these forces in perfect balance in a small-scale model, especially since fluid properties generally are the same and there are limits to the range within which soil properties can be manipulated. Testing at a range of scales is thus needed to demonstrate that the dominant processes at small scale are also dominant at large scale, and that model and prototype performance can be related to one another in a consistent way.

Despite these challenges, the testing performed thus far has provided useful insight into the erosion processes that will occur at prototype scale because similar erosion mechanisms do occur at both small and large scale, erosion-modeling equations like Eq. 1 have been shown to be valid across a range of scales, and soil and fluid properties can be reasonably estimated for use at different scales. Specifically, the submerged jet erosion test for measuring erodibility parameters of fine-grained soils can be performed over a wide range of stresses, including stresses similar to those encountered in prototype-size situations.

7. CONCLUSIONS

The first test conducted in Reclamation's new embankment breach research facility demonstrated the value of advanced imagery data collection techniques, including time lapse photos, high definition video, and photogrammetric image analysis. The structure of the flow in the developing internal erosion channel was complex and exhibited structures and details that are typically not considered in idealized mathematical models used to predict erosion rates and breach development. By incorporating these details it may be possible to improve future numerical models that simulate dam breach development. The testing performed thus far has considered only a single soil type, but the mechanisms observed may be relevant to a range of soil types that exhibit cohesive behavior and erosion by detachment-limited processes.

8. ACKNOWLEDGMENTS

This work was co-funded by the Bureau of Reclamation's Dam Safety Technology Development Program and the Nuclear Regulatory Commission, Office of Nuclear Regulatory Research.

9. REFERENCES

ASTM Standard D1556 (2015). Standard test method for density and unit weight of soil in place by sand-cone method. American Society for Testing and Materials, West Conshohocken, PA.

ASTM Standard D5852 (2007). Standard test method for erodibility determination of soil in the field or in the laboratory by the jet index method. American Society for Testing and Materials, West Conshohocken, PA.

Hanson, G.J. and Simon, A. (2001). "Erodibility of cohesive streambeds in the loess area of the midwestern USA." *Hydrological Processes*, Vol. 15, pp. 23-38.

Hanson, G.J. and Cook, K.R. (2004). "Apparatus, test procedures, and analytical methods to measure soil erodibility in situ." *Applied Engineering in Agriculture*, 20(4):455-462.

Hanson, G.J., Tejral, R.D., Hunt, S.L. and Temple, D.M. (2010). "Internal erosion and impact of erosion resistance," *Proceedings of the 30th Annual USSD Conference*, United States Society on Dams, Denver, CO.

Hassan, M., and Morris, M. (2008). "IMPACT Project Field Tests Data Analysis." Report T04-08-04. FLOODsite Project Contract No. GOCE-CT-2004-505420. (www.floodsite.net)

Lovell, A (2004). "Breach formation in embankment dams. Results from Norwegian field tests." International Seminar: Stability and Breaching of Embankment Dams, Oslo, Norway 21-22, October 2004.

Lovell, A, Vaskinn, K.A. and Valstad, T (2003). "Stability and breaching of dams. Data report number 4. Large scale field tests 2002." European IMPACT Project. Contract No. EVG1-CT-2001-00037. (www.impact-project.net)

Lovell, A. and Vaskinn, K.A. (2004). "Stability and breaching of dams. Data report number 5. Large scale field tests 2003." European IMPACT Project. Contract No. EVG1-CT-2001-00037. (www.impact-project.net)

Pugh, C.A., (1985). *Hydraulic Model Studies of Fuse Plug Embankments*. Report No. REC-ERC-85-7, Bureau of Reclamation, Denver, CO.

Wahl, T.L. and Lentz, D.J. (2011). Physical hydraulic modeling of canal breaches. Hydraulic Laboratory Report HL-2011-09, U.S. Dept. of the Interior, Bureau of Reclamation, Denver, Colorado, 56 pp.